Mon. Not. R. Astron. Soc. **276**, 651–662 (1995)

Galactic fountains as magnetic pumps

Axel Brandenburg,*[1] David Moss[2] and Anvar Shukurov[3]
[1] *Advanced Study Program & High Altitude Observatory, NCAR†, PO Box 3000, Boulder, CO 80307, USA*
[2] *Department of Mathematics, The University, Manchester M13 9PL*
[3] *Computing Center, Moscow University, Moscow 119899, Russia*

Accepted 1995 May 22. Received 1995 May 10; in original form 1994 November 29

ABSTRACT
We study a simple, kinematical model of a galactic fountain flow and show that a horizontal field in the galactic plane can be pumped into the halo to a height of several kiloparsecs. This pumping effect results from the topological structure of the flow in which the updraughts (represented by hot gas) form a connected network, whereas the downdraughts (associated with isolated cool clouds) are disconnected from each other. Such a flow traps the large-scale magnetic field in the disc and deposits it at the top of the fountain flow. Unlike previously studied models of topological pumping, in our case the flow is not constrained to a closed box and horizontal magnetic flux can leak out at the top. We find significant pumping of mean magnetic field into the halo, which can be parametrized by an advection velocity of order 1–10 km s^{-1}. The resulting magnetic field strength at a height of several kiloparsecs above the galactic plane is comparable with that at the base of the flow.

Key words: magnetic fields – MHD – ISM: magnetic fields – galaxies: haloes – galaxies: kinematics and dynamics – galaxies: magnetic fields.

1 INTRODUCTION

The hot gas produced by supernovae in the discs of spiral galaxies rises to a large height above the disc plane where it cools, undergoes thermal instability and comes back to the disc in the form of discrete dense clouds. This flow is known as the galactic fountain (Shapiro & Field 1976). The filling factor of the hot gas monotonically increases with height, so that it is plausible that, at least above a certain height, the updraughts form a connected network. Therefore, the hot gas can trap a large-scale magnetic field in the disc and carry it to the top of the fountain flow. On the other hand, the downdraughts are always disconnected from each other at any height (this is merely another way of saying that the downdraughts are in the form of individual clouds). The downdraughts are then unable to pull this field back to the disc, but rather produce only small-scale indentations and loops on a magnetic line of the large-scale field. Altogether, such a topological structure of the fountain flow, with connected updraughts and disconnected downdraughts, will result in a net upward advection of the large-scale magnetic field by the galactic fountain from the disc to the halo.

This effect is known as *topological pumping* of the large-scale magnetic field. It was first suggested by Drobyshevski & Yuferev (1974) as a mechanism of a downward transfer of magnetic field to the bottom of the convective zone of the Sun. In Bénard convection (e.g. Chandrasekhar 1961), when the updraughts are at the centres of the cells and the downdraughts around the peripheries, the updraughts are topologically disconnected from each other, whereas the downdraughts occupy a topologically connected region in a horizontal plane. As a result, a large-scale magnetic field (extending over many convection cells) is trapped by the descending flows to be advected downwards (see also Moffatt 1978). However, numerical simulations of stratified convection (Stein & Nordlund 1989; Brandenburg et al. 1990, their figs 13 and 14) indicate that this mechanism might not work deep in the Sun, because the downdraughts form a connected network only in the upper part of the convection zone, and are no longer topologically connected below a certain level (but see Rast et al. 1993). This is a consequence of the vertical density stratification that concentrates the downdraughts into narrow columns. Thus, neither updraughts nor downdraughts form a continuous network across the whole convective layer. Galactic haloes are also density stratified. The difference, however, is that here the downdraughts remain disconnected at any height while the updraughts can be connected.

It is important to realize that it is the *large-scale* magnetic field that is pumped upwards by the galactic fountain, i.e.

* Present address: Nordita, Blegdamsvej 17, DK-2100 Copenhagen Ø, Denmark.

† The National Center for Atmospheric Research is sponsored by the National Science Foundation.

the field averaged over scales much larger than the scales of individual up- and downdraughts, which are below 1–2 kpc in the horizontal direction.

Since topological pumping relies on advection of the magnetic field by the flow, it is clear that it is most efficient at large values of the magnetic Reynolds number R_m, when induction effects are stronger than effects of magnetic diffusion (Drobyshevski, Kolesnikova & Yuferev 1980; Arter 1983). According to Arter (1983), topological pumping becomes a dominant mechanism for $R_m \gtrsim 50$.

The advection time-scale from the topological pumping is rather short, being of the order of the turnover time of the flow (Drobyshevski & Yuferev 1974; Arter 1983). This effect can be expected to be important for the origin of large-scale magnetic fields in the haloes of spiral galaxies, where the kinematic time-scale for fountains is 10^7–10^8 yr. In this paper we do not aim at constructing a realistic model directly applicable to real galaxies. Our goal is merely to assess (and confirm) the potential importance of this effect in spiral galaxies and to discuss a convenient parametrization so that it could be included into models of magnetic field evolution in spiral galaxies. In this spirit, our model is strictly kinematic.

2 THE MODEL

Apart from the necessity for an appropriate topology of the flow, the central role in the theory is played by the magnetic Reynolds number $R_m = U_{max}L/\eta_t$, where U_{max} is the maximum velocity of the fountain flow, L its horizontal length-scale, and η_t the turbulent magnetic diffusivity. Thus, the model explicitly includes the velocity field of the fountain flow and the effects of turbulence on all smaller scales are described by a turbulent magnetic diffusion with $\eta_t \simeq \frac{1}{3}vl$. Here, v is the turbulent velocity and l the typical length-scale of the turbulence. Thus, we have

$$R_m \simeq 3\frac{U}{v}\frac{L}{l}. \qquad (1)$$

Estimates of U at the base of the fountain flow range from 140 km s^{-1} (Kahn & Brett 1993) to 200 km s^{-1} (Norman & Ikeuchi 1989). The typical horizontal size of the regions occupied by the hot gas in the disc can be adopted as $L \simeq 1$–2 kpc, close to that of superbubbles (Tenorio-Tagle & Bodenheimer 1988). Using standard estimates of the turbulence parameters in the disc, $v \simeq 10$ km s^{-1} and $l \simeq 100$ pc, we have $R_m \simeq 500$–1200 which is a quite optimistic estimate with regard to the efficiency of the topological pumping by the fountain flow, because this effect is expected to be efficient for $R_m \gtrsim 50$ (Arter 1983). Our estimate is, however, likely to be very much an upper limit on R_m, because in spiral galaxies the turbulent magnetic diffusivity probably increases with height (see Sokoloff & Shukurov 1990; Brandenburg et al. 1992, 1993; Poezd, Shukurov & Sokoloff 1993). To obtain a lower estimate, we take v to be equal to the sound speed in the hot ($T = 10^6$ K) gas, $v = 100$ km s^{-1}, and $l = 0.3$ kpc. This yields $R_m \simeq 10$–40. We conclude that for galactic fountains the expected value of the turbulent magnetic Reynolds number is between 10 and 1000, covering the range where the topological pumping is expected to be efficient. The 'local' value of R_m is expected to be a decreasing function of z, the coordinate perpendicular to the disc plane.

Another parameter that will be of importance below is the strength of the large-scale magnetic field at the base of the fountain flow. Since only the hot, dilute gas is involved in the flow, the relevant field strength is lower than the average value in the galactic disc. Following Kahn & Brett (1993) [see also Kahn (1991)] the large-scale magnetic field at the base of the fountain flow can be estimated as follows. The radius of a supernova remnant is $R_2 \simeq 70$ pc when it merges with other remnants to form a superbubble. The mass of gas in this volume is about 200 $M_\odot$, and the radius of the region initially occupied by this gas with a number density of 1 cm^{-3} is $R_1 \simeq 13$ pc. Assuming that the large-scale magnetic field in the interstellar medium is $B_1 \simeq 2\,\mu$G, we obtain the relevant magnetic field strength in the hot interstellar medium (HIM) from flux conservation as $B_{HIM} \simeq B_1(R_1/R_2)^2 \approx B_1/30 \approx 6 \times 10^{-8}$ G.

2.1 The velocity field

To explore the topological pumping under galactic conditions, we use a model velocity field that has the required topological properties and also satisfies mass conservation for a gas density that varies in space in a realistic manner. We consider a velocity field that is periodic in the horizontal directions and restrict our analysis to a single cell, by imposing periodic boundary conditions for magnetic field.

Our velocity field is based on Arter's (1983) velocity field (which he denoted as SSW, because it was suggested by Schmidt, Simon & Weiss 1985), which we modify in order to account for a density distribution of the form

$$\rho(z) = \frac{\rho_0}{\cosh z/z_0}\, g(x,y), \qquad (2)$$

where (x,y,z) are Cartesian coordinates (with the y-axis directed along the azimuth and z along the vertical), ρ_0 is the midplane gas density, z_0 is the scale height of the asymptotic exponential distribution of ρ at large z, and $g(x,y)$ is a certain function devised to model the density contrast between a rising hot gas and descending cold clouds. Specifically, we take

$$g(x,y) = 1 + A(\cos 2\pi x + \cos 2\pi y) \qquad (3)$$

with constant A, which is the density contrast between dense and rarefied regions. With this density distribution, the downdraughts should be placed at $(x,y) = (0,0)$ and at periodically shifted positions. In many of the runs discussed below we neglect horizontal density variations and put $A = 0$, whilst in Section 3.6 we consider the case $A = 0.4$.

We should note that this model is very simplistic: we model clouds as *columns* of descending material. We model the discrete nature of clouds by introducing a time dependence of the flow (Section 3.7).

To ensure mass conservation, $\nabla\cdot(\rho\boldsymbol{U}) = 0$, our velocity field $\boldsymbol{U}$ is defined by

$$\rho\boldsymbol{U} = \nabla\times\nabla\times S(x,y,z)\hat{\boldsymbol{z}}, \qquad (4)$$

with ρ given by equation (2), $\hat{\boldsymbol{z}}$ the unit vector in the z-direction and

$$S(x,y,z) = -Cf(z)[\cos 2\pi x + \cos 2\pi y - \tfrac{1}{12}(\cos 4\pi x + \cos 4\pi y)], \qquad (5)$$

$$f(z) = \frac{z}{\cosh^3(z/z_0)},$$

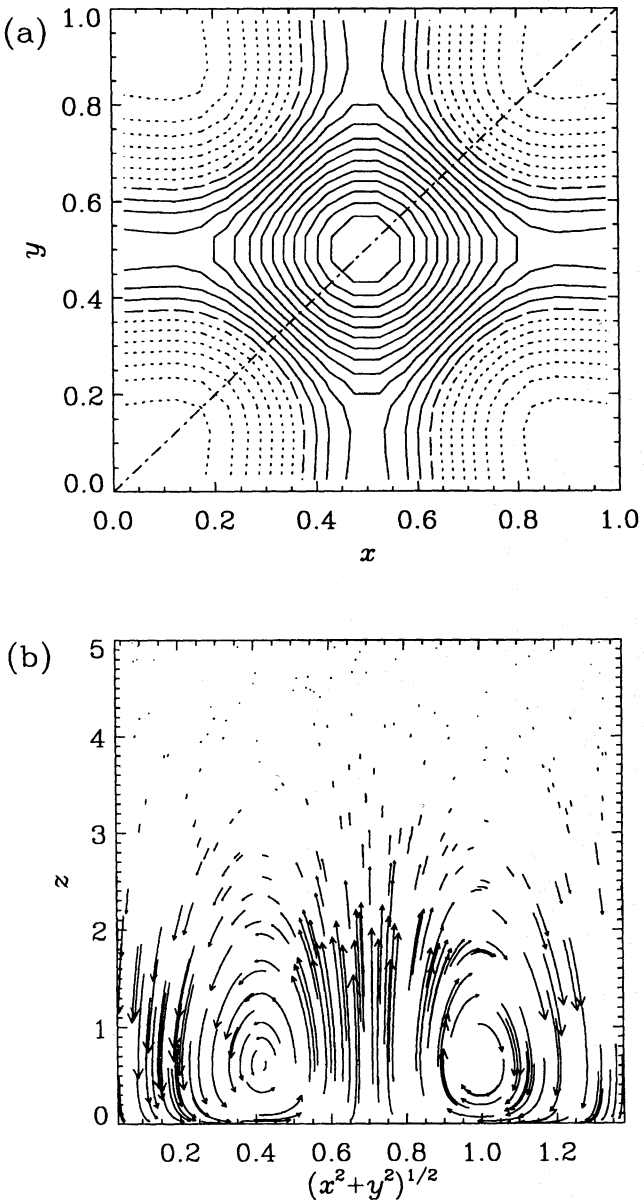

Figure 1. The velocity field (6) with $A = 0$, i.e. ρ is a function of z alone. (a) Contours of the vertical velocity in the xy plane; solid lines refer to positive U_z, dotted lines to negative U_z, and dashed lines to $U_z = 0$. (b) Projections of velocity vectors on the vertical cross-section indicated by a dashed-dotted line in (a) are shown at randomly chosen positions on this plane.

where C is a normalization constant, and the function $f(z)$ has been chosen to have $U_z = 0$ at $z = 0$ and to ensure a sufficiently rapid exponential decay of U with z at $z \gg z_0$ (the resulting exponential scale height of U is $\frac{1}{2}z_0$). Note that we adopt the opposite sign of $S(x,y,z)$ to that used by Arter (1983) in order to have connected updraughts and disconnected downdraughts, whereas Arter's velocity field has the opposite topological property.

The resulting velocity field, illustrated in Fig. 1, has isolated downdraughts centred at $(x,y) = (n,m)$ with $n,m = 0,1,\ldots$ and mutually connected updraughts. For the reader's convenience, we write out the explicit form of the velocity field [although numerical differentiation of equation (5) was used when performing the simulations described below]:

$$\begin{aligned} \boldsymbol{U} &= \frac{2\pi C}{\rho(x,y,z)} \\ &\times\{f'(\sin 2\pi x - \tfrac{1}{6}\sin 4\pi x), \\ &\quad f'(\sin 2\pi y - \tfrac{1}{6}\sin 4\pi y), \\ &\quad -2\pi f[\cos 2\pi x + \cos 2\pi y - \tfrac{1}{3}(\cos 4\pi x + \cos 4\pi y)]\}, \end{aligned} \tag{6}$$

where the prime denotes derivative with respect to z.

2.2 Basic equations

We solve numerically the induction equation,

$$\frac{\partial \boldsymbol{B}}{\partial t} = \nabla \times \left(\boldsymbol{U} \times \boldsymbol{B} - \tfrac{1}{2}\nabla\eta_t \times \boldsymbol{B} - \eta_t \nabla \times \boldsymbol{B}\right), \tag{7}$$

for the *large-scale* magnetic field with the velocity field $\boldsymbol{U}$ defined above. In equation (7) we allow for the spatial variation of the turbulent magnetic diffusivity η_t. This leads to an additional term which can be described as a field advection with the velocity $-\frac{1}{2}\nabla\eta_t$. This phenomenon is known as turbulent diamagnetism (e.g. Vainshtein & Zeldovich 1972, section II.6), and is sometimes also called *turbulent* pumping, as opposed to topological pumping, which is our main subject here. We shall investigate the effects of variable η_t in Section 3.5, but we put η_t = constant elsewhere.

The initial condition is $B_y = B_0 \exp[-(2z/z_0)^2]$ and $B_x = B_z = 0$, which describes a horizontal magnetic field initially confined to a layer whose Gaussian scale height is half the density scale height at $z \ll z_0$.

Equation (7) is solved in $0 \leqslant x \leqslant 1, 0 \leqslant y \leqslant 1, 0 \leqslant z \leqslant z_m$ with the boundary conditions

$$\begin{aligned} &\boldsymbol{B}(0,y,z) = \boldsymbol{B}(1,y,z), \quad \boldsymbol{B}(x,0,z) = \boldsymbol{B}(x,1,z), \\ &\frac{\partial B_x}{\partial z} = \frac{\partial B_y}{\partial z} = B_z = 0 \quad \text{at} \quad z = 0, \\ &B_x = B_y = 0 \quad \text{at} \quad z = z_m. \end{aligned} \tag{8}$$

The first line represents the periodicity conditions. The boundary conditions imposed at the midplane $z = 0$ single out those solutions for which the horizontal magnetic field is symmetric with respect to the midplane. At the top of the computational domain, $z = z_m$, we assume the magnetic field to be purely vertical. By virtue of the solenoidality condition, $\nabla \cdot \boldsymbol{B} = 0$, we have $\partial B_z/\partial z = 0$ at $z = z_m$. This is the simplest local boundary condition that does not restrict the horizontal magnetic flux through the computational domain. (A perfect conductor condition, which was used by Arter, would conserve horizontal magnetic flux.)

The horizontal size of the periodicity cell is taken as $L =$ 1 kpc. We measure x, y and z in units of L, U and v in $\mathrm{km\,s^{-1}}$, and, correspondingly, time in units of $1\,\mathrm{kpc}/(\mathrm{km\,s^{-1}}) \approx 1\,\mathrm{Gyr}$. The velocity field $\boldsymbol{U}$ is normalized such that $U_{\max} = 100\,\mathrm{km\,s^{-1}}$ ($C \approx 2.2$ for $A = 0$ and $C \approx 0.5$ for $A = 0.4$). We adopt a density scale height of $z_0 = 1$ kpc, which approximately equals the scale height of the Reynolds (1991) layer, and impose the boundary conditions at $z_m = 5$. We restrict z_0 and z_m to these relatively low values in order to have sufficient spatial resolution (especially near the midplane), keeping the number of uniformly distributed meshpoints in the vertical direction to an acceptable minimum of 101.

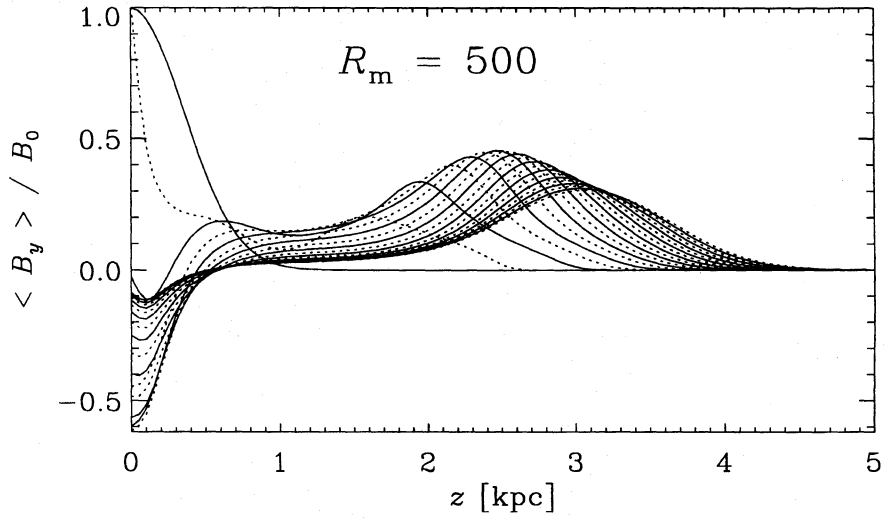

Figure 2. The horizontal magnetic field for $R_m = 500$ averaged over horizontal planes z = constant at different times, starting from $t = 0$ to $t = 1$ Gyr with an interval of 0.05 Gyr. The initial field is shown by the solid line, which is the uppermost at $z = 0$. Note that the field strength at $z > 3$ kpc monotonically increases with time during the run. The magnetic field is measured in units of the initial magnetic field at the midplane.

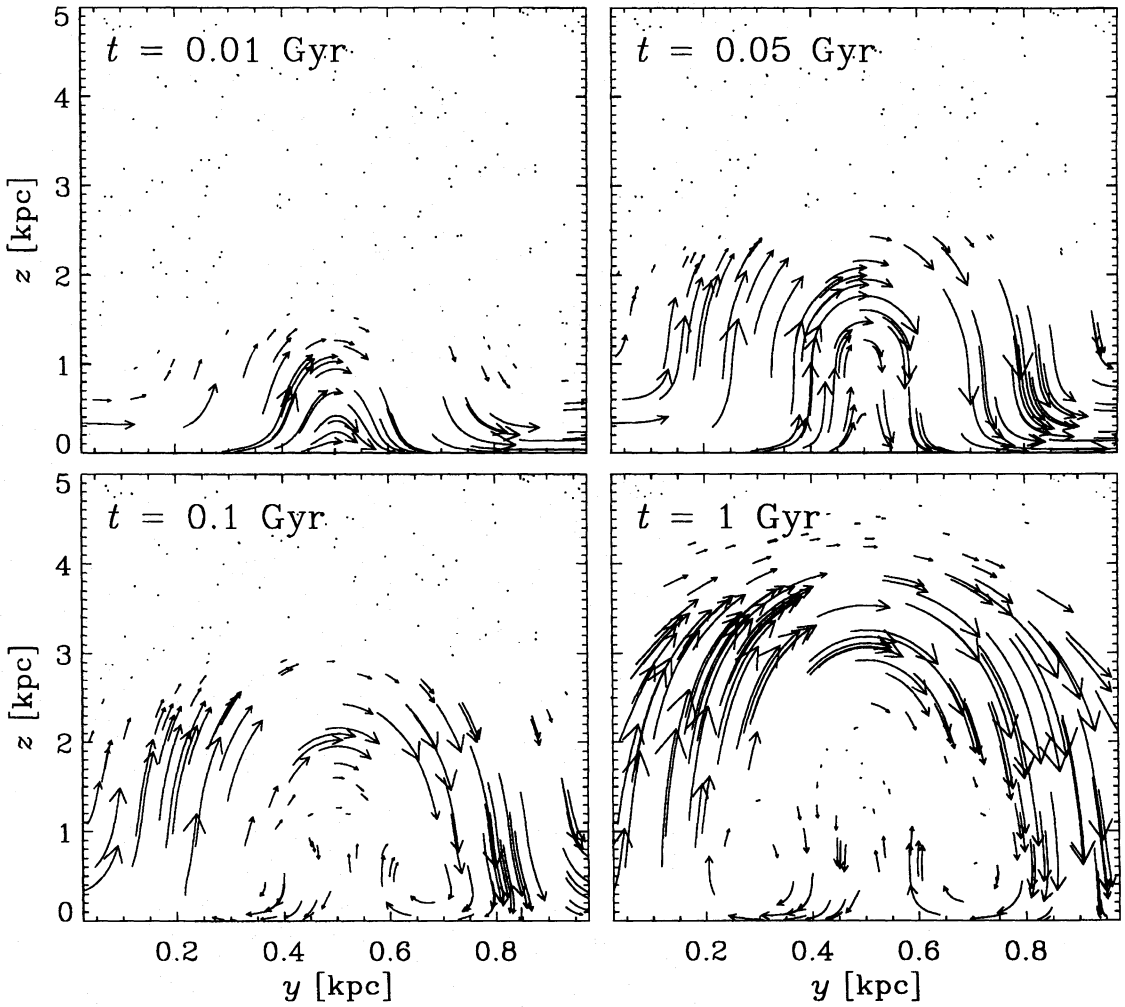

Figure 3. Snapshots of the projection of the magnetic field averaged along the x-axis on to the yz plane for $R_m = 500$, at different times. The magnetic field vectors are plotted at randomly chosen positions, with length proportional to the local magnetic field strength.

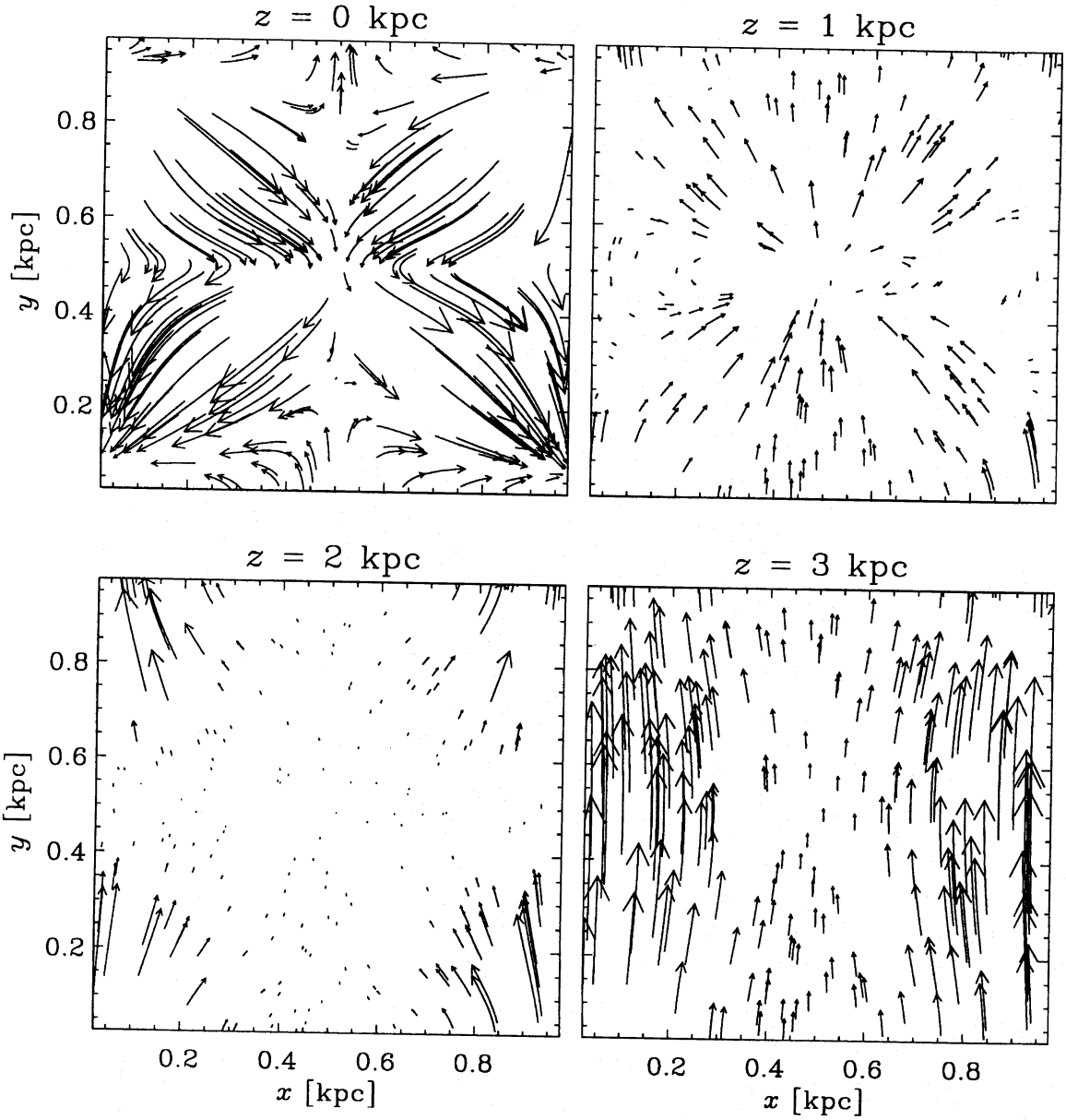

Figure 4. Snapshots of the projection of the magnetic vectors at different heights on to the xy plane, for $t = 1\,\mathrm{Gyr}$, $R_\mathrm{m} = 500$. The magnetic field is represented in the same manner as in Fig. 3.

The control parameter in our problem is R_m. Thus, our results can be easily rescaled to other values of U_max, L, z_0, and z_m by choosing an appropriate value of R_m (which is proportional to both U_max and L). The unit of time then scales with U_max/L. For example, the magnetic field distributions discussed below, which were computed for $L = 1\,\mathrm{kpc}$, $U_\mathrm{max} = 100\,\mathrm{km\,s^{-1}}$ and $z_\mathrm{m} = 5\,\mathrm{kpc}$, will be the same for $L = 2\,\mathrm{kpc}$, $U_\mathrm{max} = 200\,\mathrm{km\,s^{-1}}$, $z_\mathrm{m} = 10\,\mathrm{kpc}$ and a value of R_m that is four times larger, at the same time.

The root mean square values of the total velocity and of its z-component are very close to each other, at about $U_\mathrm{rms} = 19\,\mathrm{km\,s^{-1}}$ for $U_\mathrm{max} = 100\,\mathrm{km\,s^{-1}}$. Thus, the effective turnover time of the flow, based on its scale height $\frac{1}{2}z_0$, is $\tau = z_0/2U_\mathrm{rms} \approx 0.026\,\mathrm{Gyr}$.

Equation (7) is written for the averaged magnetic field, so that it includes the turbulent magnetic diffusivity. However, we present our results in terms of the magnetic field further averaged over horizontal planes, which we denote $\langle \boldsymbol{B} \rangle \equiv (0, \langle B_y \rangle, 0)$. (With the chosen velocity field and the initial field directed along the y-axis, $\langle B_y \rangle$ is the only non-vanishing component of $\langle \boldsymbol{B} \rangle$.) In other words, we consider turbulence and the fountain flow as two levels of small-scale motions and perform a two-step averaging to obtain physically meaningful results (cf. Drobyshevski et al. 1980).

We employ finite differences using the compact sixth-order scheme of Lele (1992) and a third-order Hyman (1979) scheme for the time step. We adopt equal mesh spacing in all three directions with the mesh interval of 0.05; thus, we have a $20 \times 20 \times 101$ mesh. This limits our magnetic Reynolds number to be below about 500.

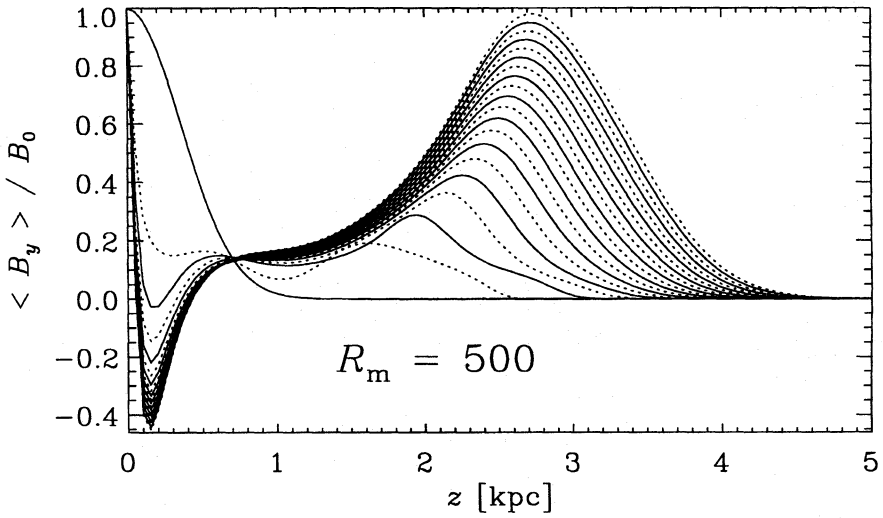

Figure 5. The same as in Fig. 2 but with a fixed magnetic field at $z = 0$. Note that now the magnetic field monotonically increases with time at $z \gtrsim 1$ kpc.

3 RESULTS

3.1 Magnetic field evolution

In Fig. 2, for $R_m = 500$ we show the y-component of the magnetic field averaged over horizontal planes as a function of z at various times. The average magnetic field is rapidly pumped to a height $z = 2$–3 kpc, where the flow velocity falls off rapidly (see Fig. 1b), and then follows a slower evolution: the magnetic 'wave' drifts towards the top until it eventually decays. The total flux of $\langle B_y \rangle$ is approximately conserved during the evolution whenever the magnetic field at the upper boundary remains small. This is true for all other runs described below.

A remarkable feature is that the average field at $z \approx 0$ even changes sign under the action of the velocity field: it is positive at $t = 0$, then becomes negative, reaching a value of about $-0.6B_0$ at $t = 0.23$ Gyr, and then slowly approaches zero. A similar reversal of the field was also noted by Drobyshevski et al. (1980) and Arter (1983). The origin of this is clearly seen from Fig. 3, indicating that it is to be associated with patches of negative horizontal flux advected to the bottom by isolated downdraughts, which appear clearly in the plots for $t = 0.1$ and 1 Gyr.

In Fig. 4, magnetic field vectors in horizontal planes are shown at various heights for $t = 1$ Gyr. One can see a striking contrast between a highly ordered magnetic pattern near the top ($z = 3$ kpc) and a complicated picture at the base. We recall that at $t = 0$ the magnetic field was ordered at $z = 0$ and negligibly small at $z \gtrsim 1$ kpc. We also see from Fig. 4 that at the top $\langle B_y \rangle$ concentrates into magnetic ropes centred above the lines connecting the downdraughts along the y-axis.

Since the magnetic field is not replenished at the bottom, and since horizontal flux is allowed to leak out at the top, the magnetic 'wave' eventually decays, so that there is no steady state with non-zero magnetic field. (We also checked this with a trial run until $t = 10$ Gyr.) However, we also computed the magnetic field evolution for the boundary condition $B_x = \partial B_z/\partial z = 0$ and $B_y = 1$ at $z = 0$, which is meant to simulate the action of a dynamo in the disc. This condition maintains a constant magnetic field at $z = 0$. Results of this experiment are presented in Fig. 5 for $R_m = 500$. Comparing this with Fig. 2, we see that the large-scale magnetic field at $z \simeq 3$ kpc becomes considerably stronger and monotonically grows with time. Even at $t = 1$ Gyr, $\langle B_y \rangle$ at $z \simeq 3$ kpc is already as strong as at $t = 0$ and it continues to grow. The drift of the secondary maximum towards larger z appears to occur at a progressively smaller rate at larger heights.

It is interesting to note that the distribution of $\langle B_y \rangle$ near $z = 0$ is rather narrow, and $\langle B_y \rangle$ changes sign not far from the midplane and again at $z \simeq 0.5$ kpc. Such a reversal of the large-scale magnetic field does not occur in the Milky Way. As we shall see below, this feature is typical only for large values of R_m. For smaller R_m the field is sign-constant: horizontal inhomogeneity of ρ and time dependence of $\boldsymbol{U}$ (Sections 3.6 and 3.7) also remove the field reversal. Thus we do not consider this to be a robust feature of our model.

3.2 Effects of varying R_m

In Fig. 6(a) we show the time evolution of the vertical distribution of the horizontal magnetic field for $R_m = 50$. As expected, the effect of the flow is weaker than for $R_m = 500$ (cf. Fig. 2). In particular, there is no field reversal at small z, and $\langle B_y \rangle$ at $z = 0$ monotonically decreases with time. However, even for this relatively small value of R_m the field strengths at $z = 0$ and $z = 2$ kpc are almost equal to each other at later times.

The value $R_m = 50$ seems to be close to the critical value for topological pumping to work (in agreement with Arter's result). For smaller values of R_m, the magnetic field evolution resembles a diffusive spread of the initially concentrated distribution. We verified this for $R_m = 20$, where the effect is weak, even though $\langle B_y \rangle$ has a secondary maximum at $z > z_0$.

In Fig. 6(b) we show the corresponding plot for $R_m = 200$, which is intermediate between the previous two cases. An immediate conclusion is that the horizontal field strength at a given height ($z > z_0$) and given time monotonically increases with R_m. In Fig. 7 we present the maximum magnetic field at $t = 1$ Gyr and the absolute maximum (with respect to both z

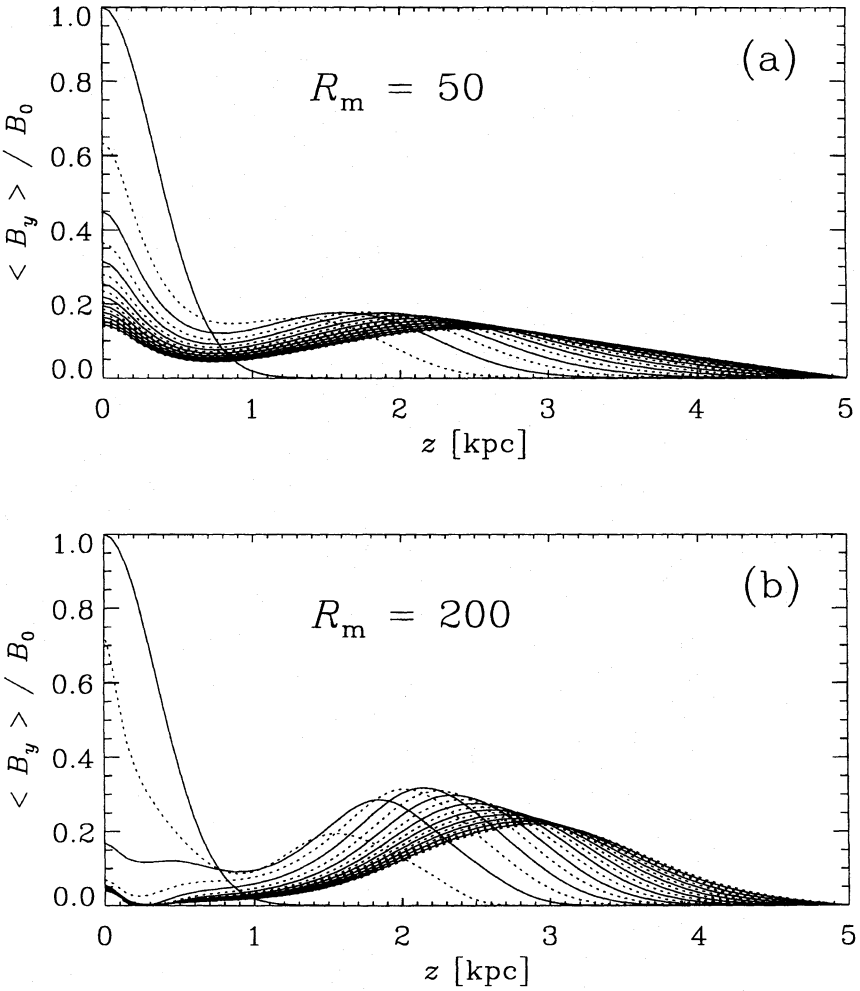

Figure 6. The same as in Fig. 2 but for (a) $R_m = 50$ and (b) $R_m = 200$.

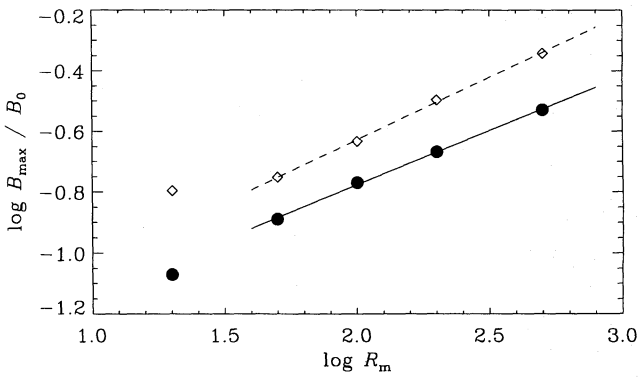

Figure 7. The maximum magnetic field at $t = 1$ Gyr (filled circles) and the absolute maximum magnetic field for $z > z_0$ and $0 < t \leqslant 1$ Gyr (open squares), as functions of R_m. Power-law fits to the data at $R_m = 50$, 100, 200 and 500 are shown by solid and dashed lines, respectively. The data at $R_m = 20$ deviate considerably from these fits.

and t) as functions of R_m. The fits shown in the figure have the form $B_{max} = aR_m^b$, which are shown by a solid line for $t = 1$ Gyr (with $a \approx 0.032$ and $b \approx 0.36$) and a dashed line for the absolute maximum (with $a \approx 0.035$ and $b \approx 0.41$). As expected, the results for $R_m = 20$ do not lie on this fit, which confirms that diffusion effects become important at this small R_m, whilst topological pumping is dominant for $R_m \gtrsim 50$.

3.3 Downward pumping

To demonstrate more clearly the topological nature of the pumping, we solve the induction equation using a velocity field with the opposite topology, i.e. with connected downdraughts and disconnected updraughts. For this purpose, we simply take the velocity field $-\boldsymbol{U}$, where $\boldsymbol{U}$ is specified by equation (6). We denote these runs by *negative* values of R_m (cf. Drobyshevski et al. 1980). In Fig. 8 we illustrate the magnetic field evolution for $R_m = -500$ in the same form as for $R_m = 500$ in Fig. 2. The result is dramatic: it can be seen that the velocity field with connected downdraughts strongly compresses the magnetic field at $z = 0$. The magnetic field is negligible at $z \gtrsim 2$ and negative at $z \simeq 1.2$, and *grows* with time at $z = 0$, whilst the width of the magnetic field distribution strongly decreases. This implies that the effects described above are connected with non-trivial topological properties of the flow.

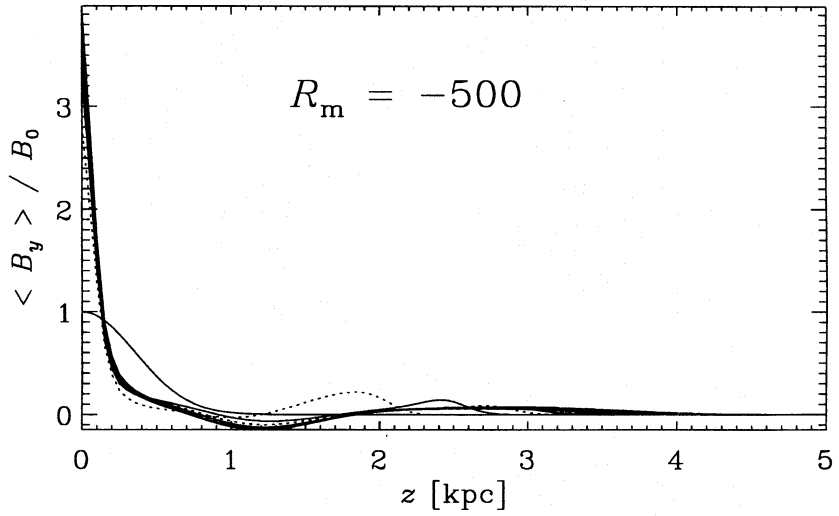

Figure 8. The downward topological pumping of magnetic field by a flow with connected downdraughts and disconnected updraughts. $R_m = -500$. The setup is the same as in Fig. 2, except for the opposite sign of R_m. The difference between Fig. 2 and this plot verifies the topological nature of the upward magnetic field advection seen in Figs 2 and 6.

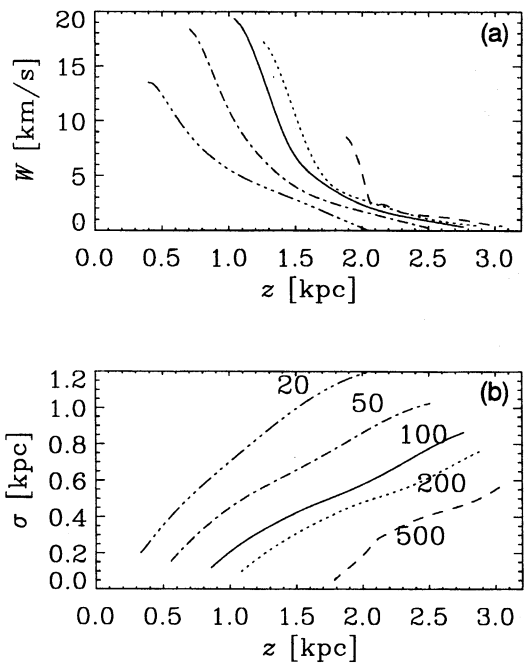

Figure 9. (a) The velocity at which the magnetic field maximum travels upwards shown as a function of z for $R_m = 20$ (dashed-triple-dotted line), 50 (dashed-dotted), 100 (solid), 200 (dotted) and 500 (dashed). (b) The half-width of the secondary maximum of the magnetic field found at large z as a function of z; the values of R_m are indicated near the corresponding curves.

3.4 Parametrization of the pumping effect

As argued by Moffatt (1974) and Drobyshevski et al. (1980), topological pumping can be described in terms of off-diagonal elements of the so-called 'α tensor' α_{ij}, defined by the relation $\mathcal{E}_i = \alpha_{ij} B_j$, where $\mathcal{E}_i$ is the i-component of the electromotive force (e.g. Krause & Rädler 1980). In this language, topological pumping can be described by a mean advection velocity $\boldsymbol{W}$, acting on the *mean*, or large-scale magnetic field, with $\alpha_{ij} = -\epsilon_{ijk} W_k$ and W being proportional to an odd power of R_m when R_m is small. This is clearly seen to be true when one inspects the time evolution of the mean magnetic field shown in Figs 2, 5 and 6. For $R_m > 0$ the field propagates towards larger z as a whole, being advected at a certain velocity (i.e. $\boldsymbol{W} = W\hat{\boldsymbol{z}}$). (Simultaneously, the width of the field distribution increases due to (turbulent) magnetic diffusion.) For $R_m < 0$ (Fig. 8), we expect that $W < 0$ and the field is indeed compressed at $z = 0$.

In Fig. 9(a) we plot the velocity W, at which the maximum of the field travels upwards, as a function of z. We only succeeded in finding a more or less reasonable fit to the rightmost parts of the curves (corresponding to relatively late times): $W \approx \tau^{-1}(z_W - z)$ with $\tau \approx 0.04 R_m^{0.50}$ and $z_W \approx 1.5 R_m^{0.13}$. Note that the curves start at certain finite heights depending on R_m. This is a manifestation of a peculiar feature of the pumping mechanism: the large-scale magnetic field is almost instantaneously (within a few turnover times) advected to a finite height and then follows a relatively slow drift.

In Fig. 9(b) we show the half-width σ of the secondary maximum of the magnetic field, which occurs at large height, as a function of z. More precisely, σ^2 is the dispersion of a Gaussian fitted to the field distribution near the maximum. The growth of σ can be naturally explained by diffusion effects. We should note only that the background turbulence alone does not determine the effective turbulent diffusivity, but that the fountain flow itself also makes a considerable contribution. The diffusive widening of the field distribution leads to $\sigma \propto t^{1/2}$. Since the maximum of the field propagates at variable speed, the dependence of σ on z is more complicated than a simple square root behaviour. When plotted as a function of t, the half-width exhibits an approximately $t^{1/2}$ behaviour for a relatively small value of R_m but again deviates from it for a larger R_m. This can be understood as an indication that the contribution of the fountain flow to the effective turbulent diffusion grows with R_m (cf. Drobyshevski et al. 1980).

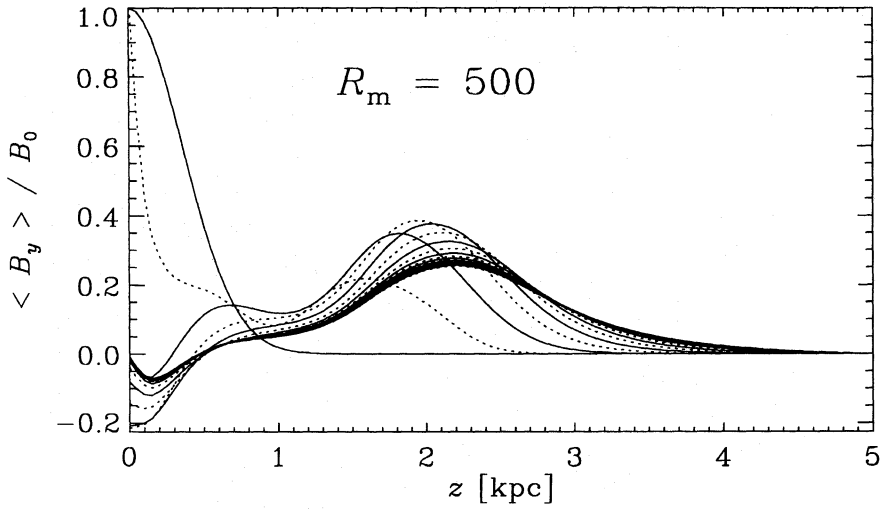

Figure 10. Topological pumping with turbulent magnetic diffusivity growing with z. The same quantities are plotted as in Fig. 2, but with η_t given by equation (9) for $R_m = 500$. Individual curves almost overlap at later times.

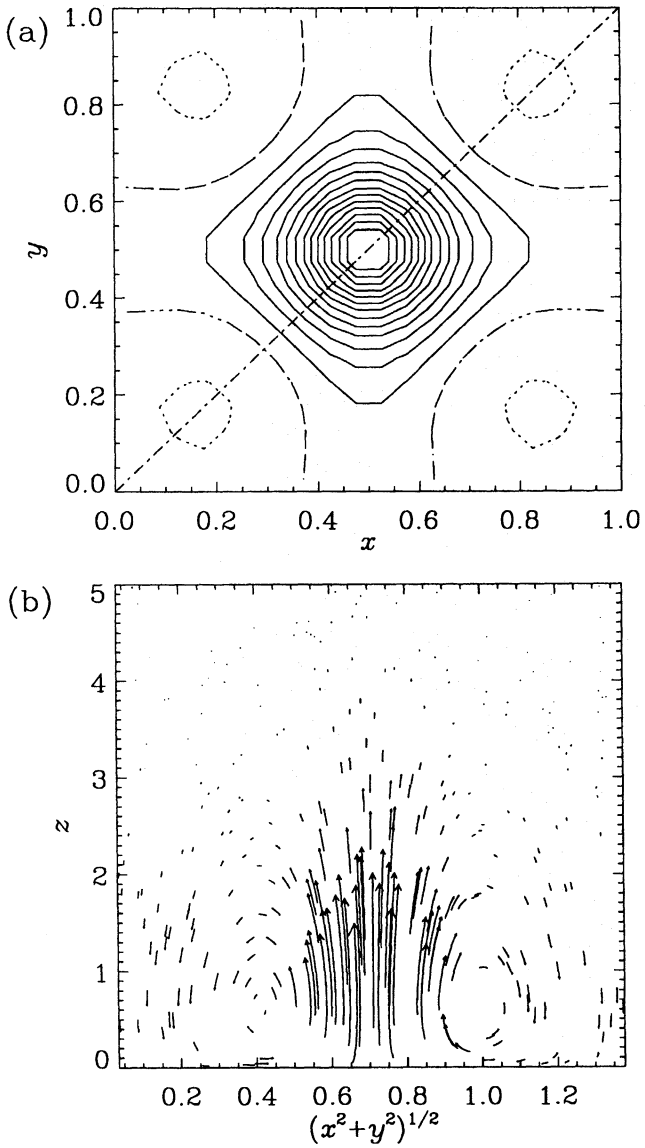

Figure 11. The same as in Fig. 1 but for a horizontally non-uniform density distribution, with $A = 0.4$ in equation (2).

3.5 Non-uniform η_t: turbulent diamagnetism

Up to now, we have considered the behaviour of the large-scale magnetic field in the galactic fountain assuming that the background turbulent magnetic diffusivity is independent of z. However, the turbulent velocity in galactic haloes grows with z, so that we expect that η_t is a growing function of z.

A variation of η_t with z brings about another effect leading to a net transport of magnetic flux along the vertical direction, known as *turbulent diamagnetism* (Zeldovich 1956): the large-scale magnetic field is advected at the velocity $V = -\frac{1}{2}\nabla\eta_t$: this is explicitly included on the right hand side of equation (7). For η_t growing with z, we have $V_z < 0$, so that the effect opposes the topological pumping.

It is clear that turbulent diamagnetism will decelerate and possibly halt the upward propagation of the magnetic field. Let us assume that

$$\eta_t = \eta_0(1 + z^2), \tag{9}$$

where η_0 is the turbulent magnetic diffusivity at the midplane, so that η_t grows by a factor of 26 over the distance $z = 5$ kpc. Then the upward propagation of the large-scale magnetic field owing to the topological pumping is balanced by the downward transport due to the turbulent diamagnetism at a height $z = W/\eta_0$. As an example, we took $\eta_0 = 0.2\,\mathrm{km\,s^{-1}\,kpc} = 6 \times 10^{26}\,\mathrm{cm^2\,s^{-1}}$. Taking $W = 0.5$–$1\,\mathrm{km\,s^{-1}}$ as a typical value of W at $z \gtrsim 3$ kpc (see Fig. 9a), we can estimate that in a quasi-steady state the large-scale magnetic field will be kept at $z \simeq W/\eta_0 = 2$–5 kpc.

To illustrate the result of the competition between the topological pumping and turbulent diamagnetism, we solved the induction equation with η_t of the form (9) and η_0 specified as in the previous paragraph. The result for $R_m = 500$ is shown in Fig. 10. It is instructive to compare Fig. 10 with Fig. 2. It is clear that turbulent diamagnetism decelerates the upward propagation of magnetic field and shifts the maximum towards smaller values of z.

3.6 Effects of dense downdraughts

In this section we briefly discuss the role of the density contrast between regions occupied by updraughts and downdraughts.

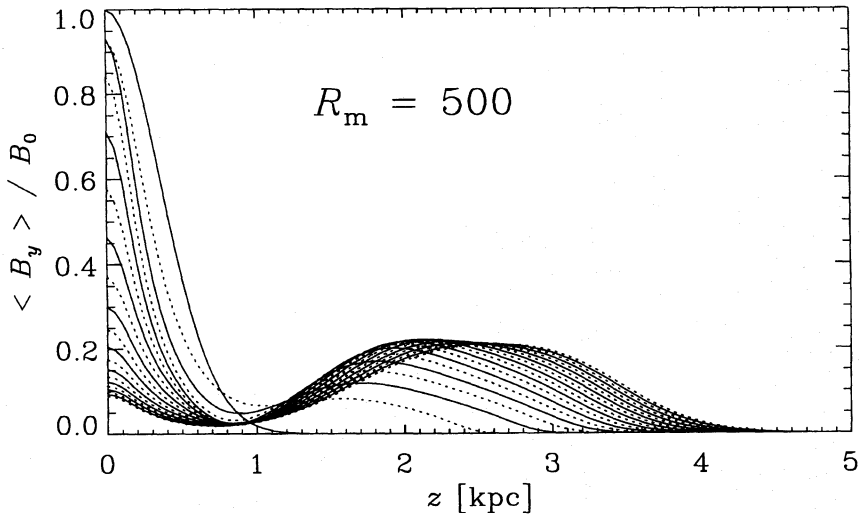

Figure 12. The same as in Fig. 2, but for a horizontally non-uniform density distribution with $A = 0.4$ in equation (2).

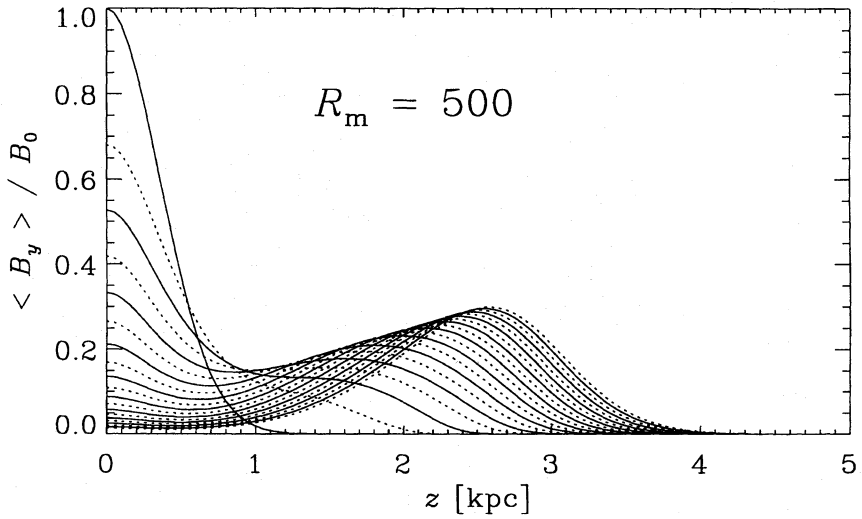

Figure 13. The same as in Fig. 2, but for a horizontally non-uniform density distribution with $A = 0.4$ in equation (2), combined with an unsteady velocity field.

In galactic fountains, this contrast arises because the gas falls back to the disc only after it has cooled and condensed into clouds. To model this, we take a horizontally non-uniform density distribution of the form (2) with $A = 0.4$ (leading to a lateral density contrast of 1:9). Since the velocity field (6) follows from mass conservation, this results in weaker downdraughts (because the area occupied by the downdraughts remains the same in our model). In Fig. 11 we illustrate the resulting velocity field in a manner similar to Fig. 1. It can be clearly seen that a horizontal non-uniformity of ρ makes the downdraughts weaker.

In Fig. 12 we show the evolution of the mean magnetic field for $A = 0.4$ and η_t = constant (to be compared with Fig. 2). The result is not entirely as expected: the pumping becomes weaker (in the sense that B_{max} is smaller) and the results obtained for $R_m = 500$ resemble more those for ρ = constant and $R_m = 200$ (see Fig. 6b). This indicates the important role of downdraughts for pumping negative flux downwards.

3.7 The effects of an unsteady velocity field

To conclude our exploratory discussion of various effects that might affect the efficiency of topological pumping, we consider a time-dependent velocity field. Our intention here is to model the discrete nature of clouds. We introduce a time dependence into the velocity field such that the downdraughts persist at any given position only for a certain interval (taken to be 0.01 Gyr, corresponding to a quarter of the turnover time), and then the whole velocity field is shifted along the line $x = y$ by 0.7 kpc. As can be seen from Fig. 13, the result of this is an enhancement of the pumping in comparison with the case of non-uniform ρ and steady $\boldsymbol{U}$. The field maximum at $z \simeq 2.5$ kpc becomes higher and narrower, and the ratio of the field at the maximum to that at $z = 0$ becomes considerably larger than in Fig. 12. Nevertheless, the unsteady velocity field produces lower values of B_{max} than does a steady one, at least for $t < 1$ Gyr.

The results of the latter two subsections apparently imply that more realistic models of topological pumping in galactic fountains might confirm that this effect is a powerful mechanism of magnetic field transfer in galactic haloes.

4 DISCUSSION

The efficiency and direction of the topological pumping are determined by the magnitude of the magnetic Reynolds number and the topology of the flow. Upward motions in the galactic fountain originate in regions occupied by the hot phase of the interstellar medium in the galactic disc. The requirement that these regions form a connected network can be formulated in the language of percolation theory (see e.g. Feder 1988, chapter 7; Vicsek 1989) as a requirement that the hot phase forms a *percolating cluster*. A percolating cluster forms only when the filling factor f of the hot gas exceeds a certain threshold. Numerical simulations of percolation on three-dimensional lattices show that this threshold is found at $f = 0.137$–0.428, depending on the lattice geometry (Nakayama, Yakubo & Orbach 1994, table 1). This range of filling factors is at the lower end of that estimated for the hot phase of the interstellar medium, which ranges from $f = 0.1$ (for the chimney model see Norman & Ikeuchi 1989; Cox 1990) to 0.7 (McKee & Ostriker 1977). We conclude that the hot phase of the interstellar medium can form a connected network, thereby acting as a magnetic pump that continuously transfers the large-scale magnetic field into the halo as described above. Starburst galaxies may provide the optimal conditions, the enhanced star formation rate giving a larger filling factor and so favouring the flow topology required for the mechanism to operate.

The situation might be different in the case of the chimney model (Norman & Ikeuchi 1989). In this model, the hot phase occupies only 10 per cent of the disc volume and therefore it does not form a percolating cluster (in other words, chimneys are *isolated* outflows). Thus, the updraughts cannot drag large-scale magnetic field into the halo. *If,* however, the downdraughts were connected, the results of Section 3.3 would apply and the large-scale magnetic field would be compressed into a thin layer in the disc. However, the latter possibility seems to be hardly plausible, because the downdraughts still occur in the form of isolated clouds for any filling factor of the hot medium.

The vertical variation of the turbulent magnetic diffusivity plays an important role in establishing a quasi-steady state of the large-scale magnetic field in the halo: this effect opposes the topological pumping in that it can prevent the outward propagation of the magnetic field beyond the upper boundary of the halo.

Altogether, we expect that the combined action of topological pumping by the galactic fountain and turbulent diamagnetism results in a relatively strong horizontal magnetic field in the halo at a height of several kiloparsecs. Since this field originates in the disc, it is clear that it has the same direction in two belts above and below the galactic plane, because this is the symmetry of the large-scale magnetic field in galactic discs.

An interesting feature of our results is the rather strong vertical magnetic field concentration in the downdraught regions (see Fig. 3). The volume average of the vertical field is, of course, zero, i.e. it does not contribute to the large-scale magnetic field. Nevertheless, such vertical fields might be of importance in explaining vertical magnetic fields in the galaxy NGC 4631 (Golla & Hummel 1994), provided that it is confirmed that the relatively high polarization of the synchrotron emission from its halo is not caused by a large-scale magnetic field, but rather arises from ordered (but anti-aligned) orientations of magnetic field vectors as in Fig. 3. This suggestion is closely related to the model of a 'spiky wind' of Elstner et al. (1995), who considered a local amplification of a vertical magnetic field by a strong vertical shear just above the galactic disc. However, our model also reveals another physical effect, namely the topological pumping.

The horizontal magnetic field produced at large heights above the disc is rather strong and, if we take our results literally, it can considerably exceed the field strength at $z = 0$. For instance, at $t = 1$ Gyr we have $B_y|_{z\approx 2.5}/B_{\rm HIM} \approx 2$ for $R_{\rm m} = 100$ and about 5 for $R_{\rm m} = 200$, where $B_{\rm HIM}$ was estimated to be about 10^{-7} G in Section 2. This result is non-trivial because the ambient density rapidly decreases with z. Of course, one should not consider these specific values of the ratio of the field strengths as reliable estimates, because for $R_{\rm m} \simeq 500$ the field evolution at $z = 0$ is complicated and $B_y|_{z=0}$ can even pass through zero. More quantitative results should await a consistent inclusion of the topological pumping effect into galactic dynamo models, which might in turn be modified by the presence of the pumping. What can be said now is that this effect is undoubtedly strong and it can profoundly affect the structure and strength of the large-scale magnetic fields in the haloes of spiral galaxies.

Topological pumping offers an attractive possibility to explain the large-scale horizontal magnetic field observed in the halo of NGC 253 (Beck et al. 1994). The measurements of the Faraday rotation measure in this galaxy (seen edge-on) indicate that the magnetic field has the same direction on both sides of the galactic plane. Such a configuration would be difficult to explain by *in situ* dynamo action in the halo, because then the horizontal field should exhibit an odd parity with respect to the midplane (Sokoloff & Shukurov 1990; Brandenburg et al. 1992). We stress that the energy density of the magnetic field produced by the dynamo is usually believed to be of the order of the kinetic energy density, which for $\rho = 1.7 \times 10^{-27}\,{\rm cm}^{-3}$ and $v = 100\,{\rm km\,s}^{-1}$ yields $\approx 1.5\,\mu$G. However, the models of Brandenburg et al. (1992) indicate considerably weaker fields in the halo. An advection of magnetic field from the disc under local flux conservation (e.g. by a galactic wind) results in very weak fields in the halo because then B scales as $\rho^{-2/3}$ decreasing down to about 10^{-8} G at $\rho = 1.7 \times 10^{-27}\,{\rm cm}^{-3}$. On the other hand, a stronger field could be the result of topological pumping of the magnetic field from the disc into the halo. Since the efficiency of topological pumping is related to the filling factor of the hot gas in the disc, it is worth noting that there is quite active star formation in NGC 253, and the filling factor is therefore indeed expected to be large.

Topological pumping leads to relatively strong magnetic fields above the disc, comparable to those at the base of the fountain flow. We stress a non-trivial aspect of this fact: the field at $z \simeq 3$ kpc is stronger than that at $z \approx 0$, even though in our simulations the density is smaller by a factor of 10. Of course, this is a result of continuous pumping by the fountain flow.

The model discussed above is purely kinematic, since we

have not included the effects of the Lorentz force on the fountain flow. A consistent analysis of the non-linear effects must await more realistic models of topological pumping in galaxies. It is clear, however, that topological pumping, if too strong, could completely destroy the dynamo in the parent galaxy provided the upper boundary is open, allowing the field to leak out of the galactic halo (as in our simulations). Given the time-scales estimated above, this is unlikely to be important, if the dynamo in the galactic disc is as strong as it usually believed to be (that is, the dynamo time-scale is 10^8–10^9 yr). On the other hand, if the rate of magnetic field regeneration is larger than the rate of its escape, or if the upward migration is halted by turbulent diamagnetism (see Section 3.5), a steady state can be reached with non-vanishing magnetic field. The steady-state strength of the magnetic field pumped by the galactic fountain can be roughly estimated from equipartition between magnetic and kinetic energy densities as $B \simeq (4\pi\rho U_{\rm max}^2)^{1/2} \approx 10^{-6}\,{\rm G}$, where $\rho \simeq 1.7 \times 10^{-27}\,{\rm g\,cm^{-3}}$ is the typical gas density in the halo. This estimate is based on the assumption that the magnetic field cannot suppress the pumping by just modifying the topology of the flow, but, instead, has to choke the fountain flow completely. Note that the mean field is predominantly horizontal which maximizes its effect on the vertical motions.

We should note that earlier pumping models with closed boundary conditions showed that the steady-state strength of magnetic field grows with magnetic Reynolds number (Drobyshevski & Yuferev 1974; Drobyshevski et al. 1980; Arter 1983). Our results, obtained with different (open) boundary conditions, seem to indicate that a steady state cannot be reached without non-linear effects, whereas $R_{\rm m}$ determines the rate of magnetic field transfer (see Section 3.4) and turbulent diamagnetism only halts the upward migration of the field maximum without preventing the growth of magnetic field strength at the field maximum.

The values of the density scale height, $z_0 = 1\,{\rm kpc}$, and the upper height of the region considered, $z_{\rm m} = 5\,{\rm kpc}$, are rather low for galactic haloes where the values $z_0 = 3\,{\rm kpc}$ and $z_{\rm m} = 10\,{\rm kpc}$ seem to be more plausible. However, our intention is only to illustrate the importance of the topological pumping under galactic conditions. Our results can be rescaled to the larger values of L, z_0 and $z_{\rm m}$, as discussed in Section 2.2.

We have deliberately omitted the effects of rotation from our analysis. If included, this would add self-excitation of magnetic field by the dynamo in the fountain flow, as discussed by Sokoloff & Shukurov (1990), Brandenburg et al. (1992) and Kahn & Brett (1993). It is, however, clear that the topological effect discussed here might strongly affect dynamo action in the disc–halo system since its time-scale, $\tau \simeq 3 \times 10^7$ yr, is significantly shorter than the conventional dynamo time-scale, $(5$–$10) \times 10^8$ yr. We thus expect that galactic fountains could significantly enhance dynamo activity in the disc–halo system of a spiral galaxy.

ACKNOWLEDGMENTS

We thank Franz Kahn for valued discussions and suggestions that triggered this investigation. AS is grateful to the Department of Mathematics of the University of Manchester and the High Altitude Observatory at NCAR for their hospitality during the work on this paper. Support from NATO grant CRG 92L273 is acknowledged. AS also acknowledges financial support from the Royal Society during his stay in Manchester, and also from the Russian Foundation for Fundamental Research (projects No. 93-02-3638 and 95-02-03724) and the International Science Foundation (grant No. MNP000).

REFERENCES

Arter W., 1983, J. Fluid Mech., 132, 25
Beck R., Carilli C.L., Holdaway M.A., Klein U., 1994, A&A, 292, 409
Brandenburg A., Nordlund Å., Pulkkinen P., Stein R.F., Tuominen I., 1990, A&A, 232, 277
Brandenburg A., Donner K.J., Moss D., Shukurov A., Sokoloff D.D., Tuominen I., 1992, A&A, 259, 453
Brandenburg A., Donner K.J., Moss D., Shukurov A., Sokoloff D.D., Tuominen I., 1993, A&A, 271, 36
Chandrasekhar S., 1961, Hydrodynamic and Hydromagnetic Stability. Clarendon Press, Oxford, Chapter II
Cox D., 1990, in Thronson H.A., Shull M., eds, The Interstellar Matter in Galaxies. Kluwer, Dordrecht, p. 181
Drobyshevski E.M., Yuferev V.S., 1974, J. Fluid Mech., 65, 33
Drobyshevski E.M., Kolesnikova E.N., Yuferev V.S., 1980, J. Fluid Mech., 101, 65
Elstner D., Golla G., Rüdiger G., Wielebinski R., 1995, A&A, 297, 77
Feder J., 1988, Fractals. Plenum Press, New York
Golla G., Hummel E., 1994, A&A, 284, 777
Hyman J.M., 1979, in Vichnevetsky R., Stepleman R.S., eds, Advances in Computational Methods for PDE's —III. Publ. IMACS, p. 313
Kahn F.D., 1991, in Bloemen H., ed., Proc. IAU Symp. 144, The Interstellar Disk-Halo Connection in Galaxies. Kluwer, Dordrecht, p. 1
Kahn F.D., Brett L., 1993, MNRAS, 263, 37
Krause F., Rädler K.-H., 1980, Mean-Field Magnetohydrodynamics and Dynamo Theory. Akademie-Verlag, Berlin; also Pergamon Press, Oxford
Lele S.K., 1992, J. Comput. Phys., 103, 16
McKee C.F., Ostriker J.P., 1977, ApJ, 218, 149
Moffatt H.K., 1974, Appendix to Drobyshevski & Yuferev (1974)
Moffatt H.K., 1978, Magnetic Field Generation in Electrically Conducting Fluids. Cambridge University Press, Cambridge, Sect. 3.12
Nakayama T., Yakubo K., Orbach R.L., 1994, Rev. Mod. Phys., 66, 381
Norman C.A., Ikeuchi S., 1989, ApJ, 345, 372
Poezd A., Shukurov A., Sokoloff D., 1993, MNRAS, 264, 285
Rast M.P., Nordlund Å., Stein R.F., Toomre J., 1993, ApJ, 408, L53
Reynolds R.J., 1991, in Bloemen H., ed., Proc. IAU Symp. 144, The Interstellar Disk-Halo Connection in Galaxies. Kluwer, Dordrecht, p. 67
Schmidt H.U., Simon G.W., Weiss N.O., 1985, A&A, 148, 191
Shapiro P.R., Field G.B., 1976, ApJ, 205, 762
Sokoloff D.D., Shukurov A., 1990, Nat, 347, 51
Stein R.F., Nordlund Å., 1989, ApJ, 342, L95
Tenorio-Tagle G., Bodenheimer P., 1988, ARA&A, 26, 145
Vainshtein S.I., Zeldovich Ya.B., 1972, Usp. Fiz. Nauk, 106, 431 (Sov. Phys. Usp., 15, 159)
Vicsek T., 1989, Fractal Growth Phenomena. World Scientific, Singapore
Zeldovich Ya.B., 1956, JETP, 31, 154 (Engl. transl. 4, 460)

This paper has been produced using the Royal Astronomical Society/Blackwell Science LaTeX style file.